

Spherical photon orbits around a Kerr black hole

Edward Teo

Department of Physics, National University of Singapore, Singapore 119260

Abstract

Two circular photon orbits are known to exist in the equatorial plane of the Kerr black hole. In this paper, we investigate so-called spherical photon orbits—orbits with constant coordinate radii that are not confined to the equatorial plane. A one-parameter class of solutions is found, which includes the circular orbits as special cases. The properties of these spherical orbits are then analyzed, with the aim of classifying them by qualitative differences in their behavior. Finally, representative orbits from each class are plotted out, including a zero-angular momentum photon orbit and one with non-fixed azimuthal direction.

I. INTRODUCTION

It is well known that light, or photons, can orbit around the Schwarzschild black hole at a constant radius. In natural units, this radius takes the value $r = 3M$, where M is the mass of the black hole. Although such an orbit is unstable, it is nevertheless important from a physical viewpoint because it defines the boundary between capture and non-capture of a cross-section of light rays by the Schwarzschild black hole (see, e.g., Ref. [1]). This boundary has played an important role in determining, for example, the optical appearance of a black hole with a thin accretion disk [2], or how the night sky would appear to an observer near a black hole or very compact star [3].

In the case of a rotating Kerr black hole, there are two circular photon orbits that could exist in the equatorial plane. One is a prograde orbit moving in the same direction as the black hole's rotation, while the other is a retrograde orbit moving against the black hole's rotation. Their radii are respectively given by [4]

$$r_1 \equiv 2M \left[1 + \cos \left(\frac{2}{3} \arccos \left(-\frac{|a|}{M} \right) \right) \right], \quad (1a)$$

$$r_2 \equiv 2M \left[1 + \cos \left(\frac{2}{3} \arccos \left(\frac{|a|}{M} \right) \right) \right], \quad (1b)$$

where a is the angular momentum per unit mass of the black hole. They fall in the range $M \leq r_1 \leq 3M \leq r_2 \leq 4M$. The fact that a prograde photon orbits the black hole at a smaller radius than a retrograde one can be attributed to the well-known Lense–Thirring effect, i.e., the dragging of inertial frames due to the black hole's rotation. This dragging would cause test objects to revolve around the black hole relative to a static observer at infinity. Thus, to such an observer, a prograde photon would have to orbit at a smaller radius to compensate for the 'extra' angular momentum acquired, while a retrograde one would have to orbit at a larger radius to compensate for the 'lost' angular momentum. Indeed, in the limit of zero rotation, these two orbits coincide at $r = 3M$, giving the single circular orbit of the Schwarzschild black hole.

Now, recall that orbits around the Schwarzschild black hole are necessarily confined to a plane passing through its center, because of the spherical symmetry of the space-time. However, the Kerr black hole space-time has only an axial symmetry (in addition to being stationary), and this raises the possibility of non-planar orbits. One could, for example, contemplate the existence of spherical photon orbits—orbital paths with constant coordinate radii

that are not necessarily confined to the equatorial plane—around the Kerr black hole. Such orbits would be a non-trivial generalization of the two circular photon orbits that lie in the equatorial plane.

At first it may seem a little surprising that such spherical orbits could even exist, but there is an interesting reason as to why they are possible. Note that an object in a spherical orbit would, in addition to moving around the black hole in the azimuthal direction, be undergoing some periodic motion in the latitudinal direction. This is only possible if there is a conserved quantity associated with motion in this direction, just as angular momentum is necessarily conserved by its rotational motion in the azimuthal direction. (This result can be seen, for example, using action-angle variables [5].) Now, because the Kerr space-time has only axial symmetry, geodesics in it should have only two constants of motion, namely energy and angular momentum. However, Carter [6] has discovered the remarkable fact that geodesics in the Kerr space-time possess a third constant of motion. It turns out that Carter’s new constant governs the motion of geodesics in the latitudinal direction, although it is not related to any obvious space-time symmetry. Thus, spherical orbits around the Kerr black hole cannot be ruled out.

Indeed, spherical *timelike* orbits were first shown to exist in the extreme ($|a| = M$) Kerr black hole by Wilkins [7], who also analyzed many of their properties in his pioneering paper. An explicit example of such an orbit, obtained by numerical integration, subsequently appeared in Ref. [8]. The extension to the case of the charged Kerr–Newman black hole was considered in Ref. [9]. Spherical orbits have also been studied in the hyper-extreme ($|a| > M$) Kerr space-time [10, 11], although this case does not admit a black hole interpretation anymore.

There has been less work done on spherical photon orbits, probably because it is known that stable orbits can only exist below the inner event horizons of the Kerr [12, 13] and Kerr–Newman [14] black holes. Nevertheless, unstable photon orbits could still exist in the exterior region of a black hole. Examples of spherical photon orbits in the hyper-extreme Kerr space-time were illustrated in Ref. [15] as a byproduct of another problem, but still they offer a tantalizing hint as to how these orbits might look like.

In this paper, we shall focus on spherical photon orbits (with positive energy) outside the event horizon of a Kerr black hole, with the aim of finding and studying all such orbits. One of the motivations for doing so is because lightlike geodesics are usually easier to treat

than timelike ones, and this case is no exception. It turns out to be possible to obtain an explicit parameterization of the class of spherical photon orbits, which was not possible for the timelike orbits in Ref. [7]. With an explicit parameterization, studying the properties of the orbits becomes much simpler, and we have been able to extend the analysis of Ref. [7] in a few directions. Eventually, of course, we hope that some of the results and experience gleaned from the lightlike case can be applied back to the timelike case. Another motivation for studying the lightlike case is simply because we find it quite amazing that photons can actually trace out such orbits around a Kerr black hole (notwithstanding the existence of Carter’s constant)!

The organization of this paper is as follows: We begin in Sec. II with a brief review of the relevant geodesic equations and how Carter’s constant affects motion out of the equatorial plane. In Sec. III, the conditions for the existence of spherical photon orbits are considered, and a class of solutions is found (which includes the two equatorial orbits in (1) as special cases). The properties of these orbits are analyzed in Sec. IV; in particular, we obtain an expression for the change in the orbit’s azimuth for every oscillation in latitude. A way to classify these orbits is then proposed, and selected orbits from each class are obtained by numerical integration and plotted out in Sec. V. The paper concludes with a short discussion.

II. EQUATIONS OF MOTION

The line element of the Kerr black hole in standard Boyer–Lindquist coordinates takes the form (see, e.g., Refs. [16–18])

$$ds^2 = -\left(1 - \frac{2Mr}{\Sigma}\right)dt^2 - 2\left(\frac{2Mr}{\Sigma}\right)a \sin^2\theta dt d\varphi + \Sigma\left(\frac{dr^2}{\Delta} + d\theta^2\right) + \frac{\mathcal{A}}{\Sigma} \sin^2\theta d\varphi^2, \quad (2)$$

where

$$\begin{aligned} \Sigma &\equiv r^2 + a^2 \cos^2\theta, \\ \Delta &\equiv r^2 + a^2 - 2Mr, \\ \mathcal{A} &\equiv (r^2 + a^2)^2 - \Delta a^2 \sin^2\theta. \end{aligned} \quad (3)$$

Here, M and a are the mass and angular momentum per unit mass of the black hole, respectively. The latter is restricted to the range $0 < |a| \leq M$, with the upper limit

corresponding to the case of extreme rotation. We shall take a to be positive without any loss of generality. The event horizons of the black hole are located at the radii

$$r_{\pm} \equiv M \pm \sqrt{M^2 - a^2}, \quad (4)$$

where $\Delta = 0$. In this paper, we shall only be interested in the region of the black hole exterior to the outer horizon, i.e., $r_+ < r < \infty$ with $-\infty < t < \infty$, $0 \leq \theta \leq \pi$ and $0 \leq \varphi < 2\pi$.

The four first-order geodesic equations governing the motion of lightlike particles in this space-time can be derived, for example, using Hamilton–Jacobi techniques [6]. They are [16–18]

$$\Delta \Sigma \dot{t} = \mathcal{A}E - 2Mr a L_z, \quad (5a)$$

$$\Sigma^2 \dot{r}^2 = E^2 r^4 + (a^2 E^2 - L_z^2 - \mathcal{Q}) r^2 + 2M \left[(aE - L_z)^2 + \mathcal{Q} \right] r - a^2 \mathcal{Q}, \quad (5b)$$

$$\Sigma^2 \dot{\theta}^2 = \mathcal{Q} - \left[\frac{L_z^2}{\sin^2 \theta} - E^2 a^2 \right] \cos^2 \theta, \quad (5c)$$

$$\Delta \Sigma \dot{\varphi} = 2Mr a E + (\Sigma - 2Mr) \frac{L_z}{\sin^2 \theta}, \quad (5d)$$

where the overdot denotes differentiation with respect to an affine parameter along the geodesic. E and L_z are constants of motion determining the particle’s energy and angular momentum about the φ -axis, respectively. They are familiar from the treatment of geodesics around the Schwarzschild black hole.

On the other hand, the new constant of motion \mathcal{Q} is Carter’s constant determining the behavior of the particle’s motion in the θ -direction. Let us briefly recall how this is so, using the method of effective potentials [16]. If we set $u = \cos \theta$, then (5c) can be rewritten as

$$\begin{aligned} \left(\frac{\Sigma}{E} \right)^2 \dot{u}^2 &= \Theta(u) \\ &\equiv Q - (Q + \Phi^2 - a^2) u^2 - a^2 u^4, \end{aligned} \quad (6)$$

where the new parameters

$$\Phi \equiv \frac{L_z}{E}, \quad Q \equiv \frac{\mathcal{Q}}{E^2} \quad (7)$$

have been introduced for convenience. The physically allowed ranges for u occur when $\Theta(u)$ is non-negative, and the boundaries of these ranges can easily be found by setting $\Theta(u)$ to zero and solving the resulting quadratic equation in u^2 . Since $\Theta(1) = -\Phi^2$ is negative in

general, we require the existence of at least one positive root $u_0^2 < 1$. We shall analyze the three cases of Q positive, negative, and zero separately.

When $Q > 0$, the only positive root is given by

$$u_0^2 = \frac{(a^2 - Q - \Phi^2) + \sqrt{(a^2 - Q - \Phi^2)^2 + 4a^2Q}}{2a^2}, \quad (8)$$

and the general shape of $\Theta(u)$ is shown in Fig. 1(a). The physically allowed range for u in this case is between $\pm|u_0|$, meaning that such orbits cross the equatorial plane repeatedly. The points of the orbit which intersect the equatorial plane are referred to as the *nodes* of the orbit [7].

When $Q < 0$, a necessary condition for the right-hand side of (6) to be non-negative (hence allowing the existence of a root) is

$$a^2 - Q - \Phi^2 > 0. \quad (9)$$

But as we shall see in the following section, this condition is rather restrictive and would serve to rule out this case, at least for the photon orbits considered in this paper. This case was also ruled out for bound timelike orbits in [7].

When $Q = 0$, the two roots are $u_0^2 = 0$ and $1 - \Phi^2/a^2$. If $\Phi^2 \geq a^2$, only the first root is relevant and the general shape of $\Theta(u)$ is shown in Fig. 1(b). But if $\Phi^2 < a^2$, both roots are relevant and the general shape of $\Theta(u)$ is plotted in Fig. 1(c). Both these cases describe equatorial orbits; however, while the first is stable under perturbations in the u -direction, the second is not. As we shall also see below, it turns out that only the first case is relevant for our photon orbits.

III. CONDITIONS FOR SPHERICAL ORBITS

The radial equation of motion (5b) can be rewritten as

$$\begin{aligned} \left(\frac{\Sigma}{E}\right)^2 \dot{r}^2 &= R(r) \\ &\equiv r^4 + (a^2 - \Phi^2 - Q)r^2 + 2M[(a - \Phi)^2 + Q]r - a^2Q. \end{aligned} \quad (10)$$

Since we are looking for spherical photon orbits with constant radius r , the conditions $R(r) = \frac{dR(r)}{dr} = 0$ must hold at this radius. These two equations can be solved simultaneously,

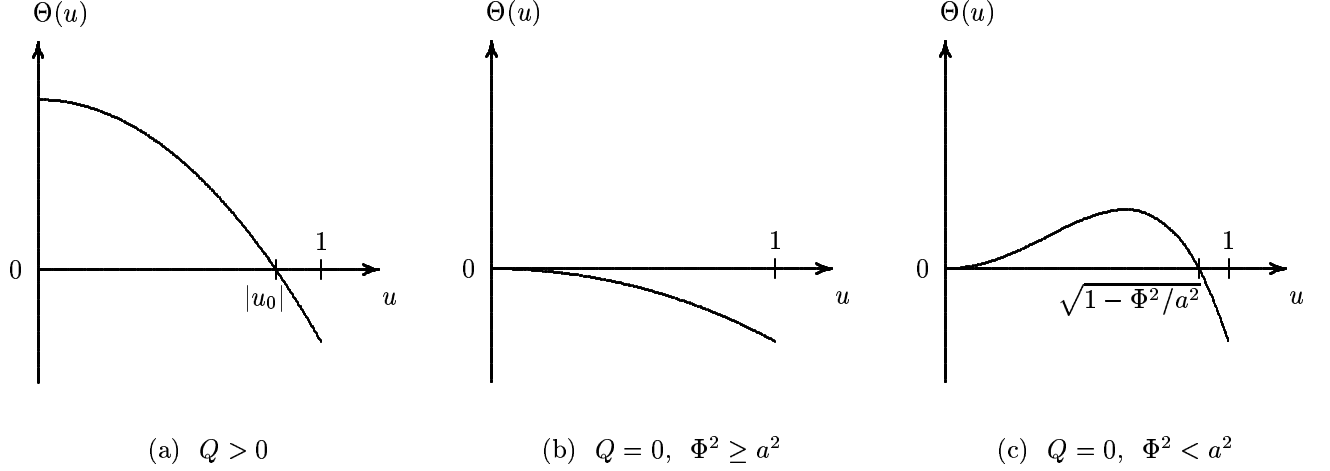


FIG. 1: Qualitative plots of $\Theta(u)$ for the cases (a) $Q > 0$; (b) $Q = 0, \Phi^2 \geq a^2$; and (c) $Q = 0, \Phi^2 < a^2$.

yielding two one-parameter classes of solutions parameterized in terms of r . They are:

$$(i) \quad \Phi = \frac{r^2 + a^2}{a}, \quad Q = -\frac{r^4}{a^2}; \quad (11a)$$

$$(ii) \quad \Phi = -\frac{r^3 - 3Mr^2 + a^2r + a^2M}{a(r - M)},$$

$$Q = -\frac{r^3(r^3 - 6Mr^2 + 9M^2r - 4a^2M)}{a^2(r - M)^2}. \quad (11b)$$

However, it should be noted that $\frac{d^2R(r)}{dr^2} > 0$ for both these classes, so if such orbits exist, they would be unstable under perturbations in the radial direction.

It turns out that Class (i) can immediately be ruled out as being unphysical. Since $Q < 0$, these parameters have to satisfy the condition (9) obtained above. However, it is not satisfied in this case, since $a^2 - Q - \Phi^2 = -2r^2 < 0$.

In the second class, Q may take either sign depending on the value of r . But note that, in general, we have

$$\begin{aligned} a^2 - Q - \Phi^2 &= -\frac{2r(r^3 - 3M^2r + 2a^2M)}{(r - M)^2} \\ &< -\frac{2r_+(r_+^3 - 3M^2r_+ + 2a^2M)}{(r - M)^2} \\ &= -\frac{2r_+^2(M^2 - a^2)}{(r - M)^2} \\ &< 0, \end{aligned} \quad (12)$$

so again (9) can never be satisfied. Thus, Class (ii) is physical only if Q is non-negative. This corresponds to a radius lying in the range $r_1 \leq r \leq r_2$, where r_1 and r_2 are the two

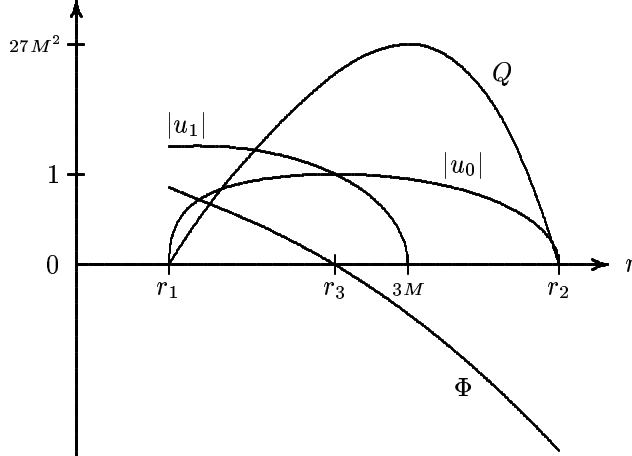


FIG. 2: Qualitative plots of Q , Φ , $|u_0|$ and $|u_1|$ versus r for solutions of Class (ii).

radii at which Q vanishes. They are none other than the radii of the equatorial orbits given by (1). From (12), we also see that $a^2 < \Phi^2$ and so these equatorial orbits are stable (c.f. Fig. 1(b)).

In the case of extreme rotation, $a = M$, Class (ii) simplifies to

$$(ii') \quad \Phi = -\frac{r^2 - 2Mr - M^2}{M}, \quad Q = -\frac{r^3(r - 4M)}{M^2}. \quad (13)$$

Again, r is bounded from above by $r_2 = 4M$. On the other hand, the lower limit $r_1 = M$ appears to coincide with the location of the event horizon itself. However, there is actually a non-zero proper distance separating the equatorial photon orbit at r_1 and the event horizon r_+ , even though they share the same coordinate radius. As explained in Ref. [4], this is due to the fact that an infinite throat develops near the horizon of the extreme Kerr black hole, which is most readily seen with the aid of an embedding diagram (c.f. Fig. 2 in Ref. [4]).

IV. PROPERTIES OF THE SPHERICAL ORBITS

In this section, we shall study in detail the properties of the spherical photon orbits of Class (ii), in the physical range $r_1 < r < r_2$. It will become apparent that such orbits exhibit a much richer set of behavior than their purely equatorial counterparts.

We begin with a discussion of the parameter Q . Its qualitative dependence on r is shown in Fig. 2. As can be seen, it monotonically increases from zero at $r = r_1$, to a maximum value of $27M^2$ at $r = 3M$, before monotonically decreasing back to zero at $r = r_2$. A

possible physical interpretation of this parameter may be obtained by setting $\theta = \frac{\pi}{2}$ in (5c). We obtain the equation $r^2\dot{\theta} = \pm\sqrt{Q}$, which shows that Q is related to the angular speed of the photon passing through the equatorial plane in the θ -direction. When $Q = 0$, the photon's motion lies entirely within the equatorial plane, just as we have deduced above. As Q increases, the photon acquires a velocity in the θ -direction as well. At the maximum value $Q = 27M^2$, the photon's motion is entirely in the θ -direction, with no component in the φ -direction. This can be confirmed by checking that $\dot{\varphi} = 0$ when $\theta = \frac{\pi}{2}$, using (5d).

On the other hand, the parameter Φ is related to the angular momentum of the photon about the φ -axis. It monotonically decreases from some positive value at $r = r_1$, to some negative value at $r = r_2$. In particular, it vanishes at the intermediate radius

$$r_3 \equiv M + 2\sqrt{M^2 - \frac{1}{3}a^2} \cos\left(\frac{1}{3} \arccos \frac{M(M^2 - a^2)}{(M^2 - \frac{1}{3}a^2)^{\frac{3}{2}}}\right), \quad (14)$$

corresponding to a photon with *zero* angular momentum. There is, in fact, a relationship between $|\Phi|$ and the maximum latitude $|u_0|$, given by (8), that the photon can reach. Observe from Fig. 2 that the latter depends inversely on the former, a result expected from the conservation of angular momentum: the smaller the angular momentum of the photon, the closer to the φ -axis it can approach. This translates into a higher latitude $|u_0|$. The photon can reach the φ -axis at its maximum latitude $|u_0| = 1$, if and only if Φ vanishes.

Since the orbits considered here vary periodically in latitude, it is useful to have a measure of this periodicity. One possibility is to consider the change in azimuth $\Delta\varphi$ for a complete latitudinal oscillation of the orbit. It turns out to be possible to obtain an exact expression for $\Delta\varphi$ for the lightlike orbits under consideration, following the timelike case [7], as we now briefly describe.

If we set $w = u^2$, then from (5d) and (6), we have

$$\frac{d\varphi}{dw} = \left[\frac{2Mra - a^2\Phi}{2\Delta} + \frac{\Phi}{2(1-w)} \right] \frac{1}{Y(w)}, \quad (15)$$

where

$$Y^2(w) \equiv Qw - (Q + \Phi^2 - a^2)w^2 - a^2w^3. \quad (16)$$

It would be useful to write the latter in the form $-a^2w(w - w_+)(w - w_-)$, where w_{\pm} are the positive and negative roots of $Y^2(w)$, respectively. Then the change in azimuth for one complete oscillation in latitude is

$$\Delta\varphi = \frac{4Mra - 2a^2\Phi}{\Delta} \int_0^{\omega_+} \frac{dw}{Y(w)} + 2\Phi \int_0^{\omega_+} \frac{dw}{(1-w)Y(w)}. \quad (17)$$

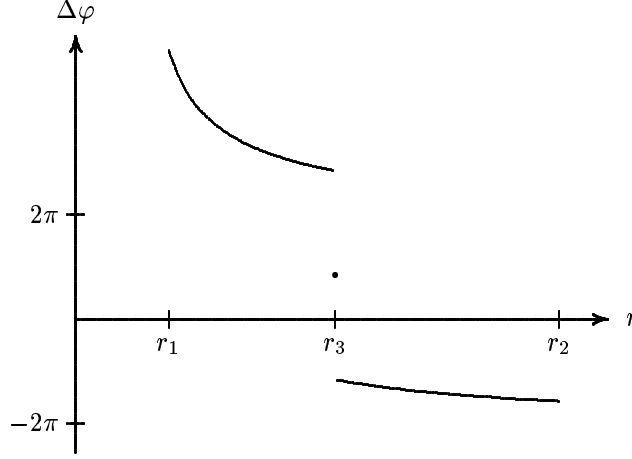


FIG. 3: Qualitative plot of $\Delta\varphi$ versus r . Orbits with $\Delta\varphi > 0$ are prograde, while those with $\Delta\varphi < 0$ are retrograde. Note the discontinuity at $r = r_3$, where $\Delta\varphi$ takes the value indicated by the single point.

These integrals can be evaluated using standard techniques, to give

$$\Delta\varphi = \frac{4}{\sqrt{w_+ - w_-}} \left[\frac{2Mr - a\Phi}{\Delta} K\left(\sqrt{\frac{w_+}{w_+ - w_-}}\right) + \frac{\Phi}{a} \frac{1}{1 - w_+} \Pi\left(-\frac{w_+}{1 - w_+}, \sqrt{\frac{w_+}{w_+ - w_-}}\right) \right], \quad (18)$$

where $K(x)$ and $\Pi(\nu, x)$ are the complete elliptic integrals of the first and third kind, respectively.

The qualitative dependence of $\Delta\varphi$ on r is shown in Fig. 3. When $r_1 < r < r_3$, corresponding to positive Φ , we see that $\Delta\varphi$ is also positive. On the other hand, when $r_3 < r < r_2$, corresponding to negative Φ , we see that $\Delta\varphi$ is negative. Thus, the orbits are prograde whenever Φ is positive, and retrograde whenever Φ is negative.

Furthermore, it can be shown that $\Delta\varphi > 2\pi$ for the prograde orbits, and $|\Delta\varphi| < 2\pi$ for the retrograde ones. This means that each latitudinal oscillation of a prograde orbit takes *more* than one revolution in φ to complete, while each latitudinal oscillation of a retrograde orbit takes *less* than one revolution in φ to complete. In either case, the nodes of the orbit are dragged in the direction of the black hole's rotation, and is a manifestation of the Lense–Thirring effect. A similar phenomenon occurs for spherical timelike orbits [7].

Note that there is a discontinuity at $r = r_3$ ($\Phi = 0$), in going from prograde to retrograde orbits. The difference between the left and right limits is, remarkably, always equal to 4π . Furthermore, the particular orbit with $\Phi = 0$ will have a positive value of $\Delta\varphi$ that lies

exactly halfway between these two limits. It turns out that there is a satisfying explanation for this behavior, which we will return to in the following section when we give an explicit example of such an orbit.

Although each orbit that we are considering has a definite non-zero value for $\Delta\varphi$, it is not guaranteed that the photon is moving in a fixed azimuthal direction at every point of its orbit. In fact, it follows from (5d) that $\dot{\varphi}$ changes sign whenever u^2 reaches the value

$$\begin{aligned} u_1^2 &\equiv \frac{2Mra - (2Mr - r^2)\Phi}{2Mra - a^2\Phi} \\ &= \frac{r^2(3M - r)}{a^2(r + M)}. \end{aligned} \tag{19}$$

A plot of $|u_1|$ can be found in Fig. 2. Note that this effect is only physically relevant if $|u_1| < |u_0|$. It can be checked that this occurs only when $r_3 < r < 3M$ (corresponding to $-2a < \Phi < 0$). Orbits with these parameters would therefore not be moving in a fixed azimuthal direction, although the net change in azimuth for one latitudinal oscillation is still negative. An example of such an orbit will also be given in the following section, together with a physical interpretation of this effect.

V. EXAMPLES OF SELECTED ORBITS

It follows from the analysis in the preceding section, and in particular from the graphs in Fig. 2, that our one-parameter class of spherical photon orbits can be divided into three sub-classes exhibiting qualitatively different behavior. Firstly, they can be categorized into prograde and retrograde orbits, depending on whether the radius r of the orbits lies between r_1 and r_3 , or between r_3 and r_2 . The sub-class of retrograde orbits can then be further divided into those without a fixed azimuthal direction ($r_3 < r < 3M$) and those with ($3M < r < r_2$). There are two special cases, namely the orbits with $r = r_3$ and $3M$.

In this section, we shall present explicit examples of spherical photon orbits from each of these three sub-classes, as well as the two special cases. These orbits can only be obtained numerically, by integrating the first-order differential equations (5a)–(5d). Fortunately, it is relatively easy to do so using standard algorithms, such as the fourth-order Runge–Kutta method [19] that we chose to use. A sufficiently small step-size was chosen so that the computed values of $\Delta\varphi$ and $|u_0|$ agreed with those obtained from the exact expressions (18) and (8) *to at least five significant figures*. This is a good consistency check that our

TABLE I: Parameters of the spherical-photon-orbit examples considered in Sec. V

Φ/M	r/M	Q/M^2	$ u_0 $	$\Delta\varphi$
0	$1 + \sqrt{2}$	$11 + 8\sqrt{2}$	1	3.1761
-1	$1 + \sqrt{3}$	$12 + 8\sqrt{3}$	0.98186	-3.7138
-2	3	27	0.93515	-4.0728
-6	$1 + 2\sqrt{2}$	$-13 + 16\sqrt{2}$	0.46335	-4.7450
1	2	16	0.97174	10.843
1.999	1.0316	3.2590	0.69543	159.42

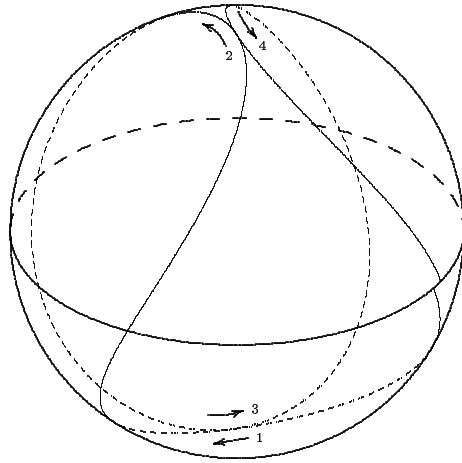


FIG. 4: Two latitudinal oscillations of the photon orbit with $\Phi = 0$. The orbit begins at the equator and heads southwards. For clarity, numbered arrows indicate the order and direction of motion.

algorithm was implemented correctly.

For simplicity, we shall only consider the case of an extreme Kerr black hole, i.e., when $a = M$. Orbits for $a < M$ turn out to be qualitatively similar.

In each of the following examples, we plot the orbits on an imaginary sphere of fixed radius. (Actual values of the radii, as well as other parameters of the orbits, may be found in Table I.) Each orbit begins at the equator and heads southwards. The observer is assumed to be located at infinity, 30° west of the starting point of the orbit, and 60° north of the equator. The sense of rotation of the black hole itself is from west to east.

We begin with the special case $\Phi = 0$ (corresponding to $r = r_3$), which describes a

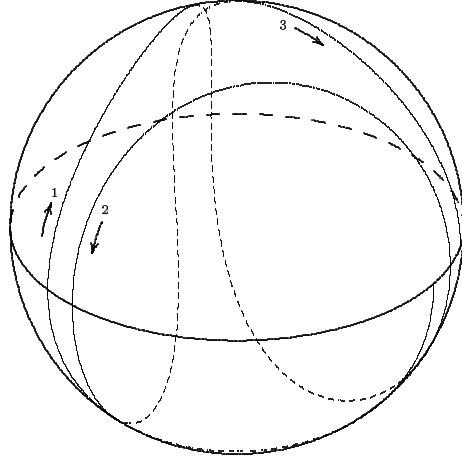


FIG. 5: Three latitudinal oscillations of the photon orbit with $\Phi = -2M$.

photon with zero angular momentum. Despite this, such a photon can still orbit the black hole at constant radius due to the dragging of inertial frames around it, as predicted by the Lense–Thirring effect. Furthermore, since $\Phi = 0$, the photon’s orbit will take it through all possible latitudes, to the φ -axis itself. Fig. 4 shows two latitudinal oscillations of this orbit. As can be seen, the photon passes alternately through the north and south poles in a prograde orbit, taking slightly more than half a revolution in φ to complete one oscillation in latitude.

Recall that this is also the case which straddles the discontinuity in the graph of Fig. 3. With an explicit visualization of such an orbit at hand, it is quite easy to understand why this discontinuity arises. Let us consider perturbing the orbit in Fig. 4 slightly away from $\Phi = 0$, in both the positive and negative directions, and examine what happens to the photon orbit near the north and south poles. It can be seen that for small positive Φ , the photon would ‘swing around’ the poles, instead of passing directly through them, in a prograde orbit. Observe that this swinging around the poles would add an extra 2π to $\Delta\varphi$, thus giving rise to a finite discontinuity in the graph of $\Delta\varphi$. On the other hand, for small negative Φ , the photon would miss the poles in a retrograde orbit. Since the orbit is now retrograde, its change in azimuth should be measured from the opposite direction; furthermore, it should be negative by definition. This effectively means we have to subtract 2π from $\Delta\varphi$.

Our next example, $\Phi = -2M$ ($r = 3M$), is also special in the sense that it is the unique orbit which has the maximum allowed value of Q , namely $27M^2$. Recall that this implies

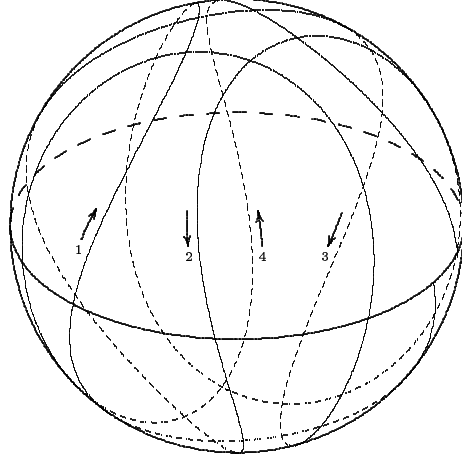


FIG. 6: Five latitudinal oscillations of the photon orbit with $\Phi = -M$.

that the photon is moving vertically whenever it is at the equator, a fact that is clear from the plot of the orbit in Fig. 5. On the whole, however, it is still a retrograde orbit with negative angular momentum. This behavior can be understood from the Lense–Thirring effect: the dragging of inertial frames is strongest at the equator, and in this case, it precisely cancels out the retrograde motion of the photon. Away from the equator, the dragging becomes weaker and so the orbit regains its retrograde character.

It was shown in the preceding section that when $-2M < \Phi < 0$ ($r_3 < r < 3M$), the photon orbits do not have a fixed azimuthal direction. Five latitudinal oscillations for the case $\Phi = -M$ is plotted in Fig. 6. Observe that although the orbit is retrograde on the whole, it is actually moving in the *positive* φ -direction within a certain latitude ($|u_1| = 0.73205$) of the equator. This can again be attributed to the strength of the Lense–Thirring effect in the equatorial region: in this case, the negative angular momentum of the photon is *not* large enough to negate this effect, resulting in it being dragged along in the direction of the black hole’s rotation.

For angular momentum $-7M < \Phi < -2M$ ($3M < r < r_2$), the orbits are completely retrograde even in the equatorial region. This is due to the fact that the angular momentum of the photon is large enough in this case to dominate over the Lense–Thirring effect. A representative example of $\Phi = -6M$ is shown in Fig. 7. Another point to note from this figure, is the relatively low maximum latitude ($|u_0| = 0.46335$) of the photon. It goes to zero in the limit $\Phi \rightarrow -7M$, resulting in a retrograde circular orbit in the equatorial plane.

We now briefly turn to the case when Φ is positive: $0 < \Phi < 2M$ ($r_1 < r < r_3$),

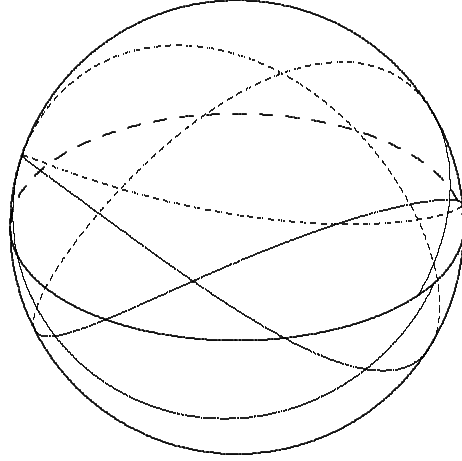


FIG. 7: Four latitudinal oscillations of the photon orbit with $\Phi = -6M$.

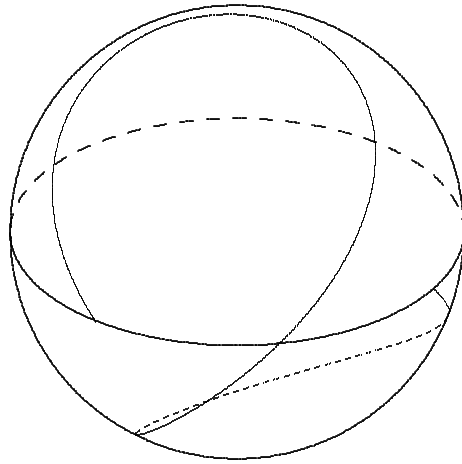


FIG. 8: One latitudinal oscillation of the photon orbit with $\Phi = M$.

corresponding to prograde orbits. Consider, for example, the orbit with $\Phi = M$ as illustrated in Fig. 8. The photon swings right around both the south and north poles, taking more than one revolution in φ to complete one oscillation in latitude. Another example is given in Fig. 9 for the more extreme case of $\Phi = 1.999M$. A helical pattern is apparent in this case, similar to the timelike example in Fig. 6 of Ref. [7]. The angle of inclination of the photon (recall that this is related to Q when the photon is at the equator) is now so small that it takes more than 25 revolutions just to complete one oscillation in latitude.

The alert reader may, at this stage, be wondering why the orbit in Fig. 9 does not appear to be approaching the circular orbit that is supposed to exist when $\Phi = 2M$. This is due to the fact that for the extreme Kerr black hole, the prograde circular orbit no longer belongs

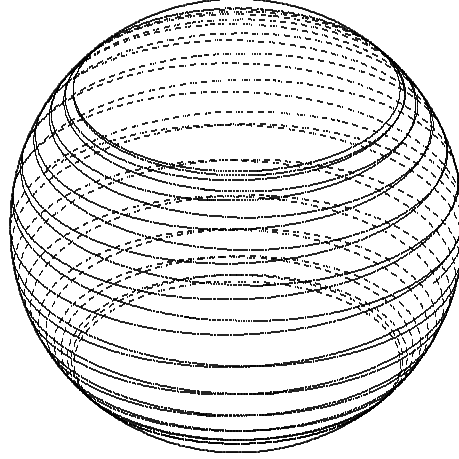


FIG. 9: One latitudinal oscillation of the photon orbit with $\Phi = 1.999M$. For clarity, the circle indicating the equator has been removed from this and the subsequent figures.

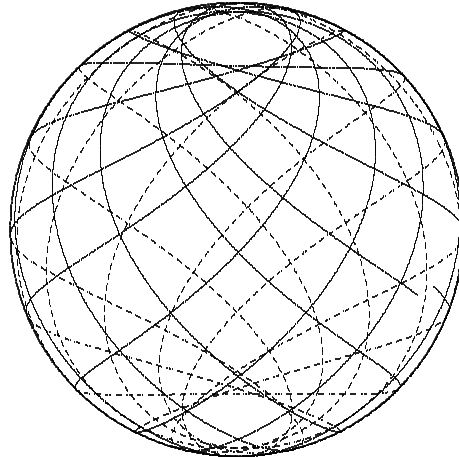


FIG. 10: Eleven latitudinal oscillations of the photon orbit with $\Phi = M$.

to the class of solutions (13) (even though the retrograde one does, as mentioned above). In fact, it can be seen from (13) that as $r \rightarrow r_1$, Q approaches the non-zero constant $3M^2$. This subtlety is only present when the limit of extreme rotation is taken.

Finally, we remark that rather interesting quasi-periodic patterns would result if the photon orbits are continued for many latitudinal oscillations. For example, Fig. 10 shows how the photon orbit with $\Phi = M$ in Fig. 8 would look like after eleven latitudinal oscillations. The existence of a maximum latitude is manifest as circles surrounding the north and south poles. Fig. 11 shows how the orbit with $\Phi = -6M$ in Fig. 7 would appear after a total of 49 latitudinal oscillations. Because of its relatively low maximum latitude, the orbit appears as

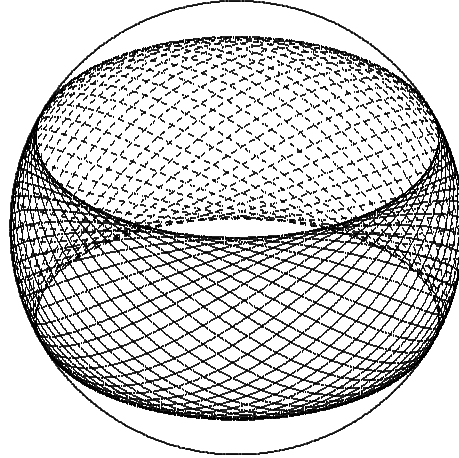


FIG. 11: 49 latitudinal oscillations of the photon orbit with $\Phi = -6M$.

a ‘band’ surrounding the equator. The orbit will fill up the area of the band as time passes.

We have written a Java applet to plot the spherical photon orbits considered in this section (as well as other examples) as wireframe models, which the user can then interactively rotate to view them from any angle. They are available at the World Wide Web site <http://www.physics.nus.edu.sg/~phyteoe/kerr/>.

VI. CONCLUSION

While it is well known that two circular photon orbits can exist in the equatorial plane of the Kerr black hole, it is less generally appreciated that spherical photon orbits extending beyond the equatorial plane are also possible. In this paper, we have found a one-parameter class of solutions describing spherical photon orbits outside the black hole horizon, and analyzed their properties. As we have seen, these orbits exhibit a variety of interesting behavior that are absent in circular orbits. Finally, representative examples of such orbits were obtained numerically, and used to illustrate some of these behavior.

Perhaps the biggest drawback of these spherical photon orbits is the fact that they are unstable under radial perturbations. This is, however, not a problem for the spherical timelike orbits considered by Wilkins [7]; moreover, timelike orbits would be more relevant than lightlike ones from an astrophysical viewpoint. Although a fairly detailed study of these orbits was already performed by him, more remains to be done. One of these is to extend his analysis to the non-extremal case. Another is to categorize all the possible orbits and

their defining properties (only the helical case was explicitly described in Ref. [7]), perhaps along the lines of this paper. For instance, what other general shapes can the orbits take besides helices? How do zero-angular momentum orbits behave? Are orbits with non-fixed azimuthal direction possible? These are but some of the questions that deserve further attention.

Acknowledgments

I would like to thank Ang Koon Liang for his collaboration at the initial stages of this work.

-
- [1] Martin, J. L. (1996). “General relativity: a first course for physicists”, revised ed., Prentice Hall, London, pp. 121–123.
 - [2] Luminet, J.-P. (1979). “Image of a spherical black hole with thin accretion disk”, *Astron. Astrophys.* **75**, 228–235.
 - [3] Nemiroff, R. J. (1993). “Visual distortions near a neutron star and black hole”, *Am. J. Phys.* **61**, 619–632.
 - [4] Bardeen, J. M., Press, W. H., and Teukolsky, S. A. (1972). “Rotating black holes: locally nonrotating frames, energy extraction, and scalar synchrotron radiation”, *Astrophys. J.* **178**, 347–369.
 - [5] Goldstein, H. (1980). “Classical mechanics”, 2nd ed., Addison-Wesley, Reading, Mass., pp. 457–462.
 - [6] Carter, B. (1968). “Global structure of the Kerr family of gravitational fields”, *Phys. Rev.* **174**, 1559–1571.
 - [7] Wilkins, D. C. (1972). “Bound geodesics in the Kerr metric”, *Phys. Rev. D* **5**, 814–822.
 - [8] Goldstein, H. (1974). “Numerical calculation of bound geodesics in the Kerr metric”, *Z. Phys.* **271**, 275–279.
 - [9] Johnston, M. and Ruffini, R. (1974). “Generalized Wilkins effect and selected orbits in a Kerr–Newman geometry”, *Phys. Rev. D* **10**, 2324–2329.

- [10] Izmailov, S. V. and Levin, E. S. (1979). “The determination of the parameters of “spherical” motion in a Kerr field”, *Sov. Phys. J.* **22**, 472–478.
- [11] Izmailov, S. V. and Levin, E. S. (1981). “On a class of stable “spherical” configurations in the Kerr field”, *Sov. Phys. J.* **23**, 645–648.
- [12] Calvani, M. and de Felice, F. (1978). “Vortical null orbits, repulsive barriers, energy confinement in Kerr metric”, *Gen. Rel. Grav.* **9**, 889–902.
- [13] Stuchlik, Z. (1981). “The radial motion of photons in Kerr metric”, *Bull. Astron. Inst. Czechosl.* **32**, 40–52.
- [14] Calvani, M., de Felice, F., and Nobili, L. (1980). “Photon trajectories in the Kerr–Newman metric”, *J. Phys. A: Math. Gen.* **13**, 3213–3219.
- [15] Schastok, J., Soffel, M., Ruder, H., and Schneider, M. (1987). “Stellar sky as seen from the vicinity of a black hole”, *Am. J. Phys.* **55**, 336–341.
- [16] Stewart, J. and Walker, M. (1973). “Black holes: the outside story”, *Springer Tracts in Modern Physics, Vol. 69* Springer, Berlin, pp. 69–115.
- [17] Sharp, N. A. (1979). “Geodesics in black hole space-times”, *Gen. Rel. Grav.* **10**, 657–670.
- [18] Dymnikova, I. G. (1986). “Motion of particles and photons in the gravitational field of a rotating body”, *Sov. Phys. Usp.* **29**, 215–237.
- [19] Press, W. H., Flannery, B. P., Teukolsky, S. A., and Vetterling, W. T. (1993). “Numerical recipes in C”, Cambridge University Press, Cambridge, pp. 710–714.